

Two- and three-dimensional simulations of the phase separation of elastically coherent binary alloys subject to external stresses

Daniel Orlikowski,¹ Celeste Sagui,¹ Andrés M. Somoza,² and Christopher Roland¹

¹*Department of Physics, North Carolina State University, Raleigh, North Carolina 27695*

²*Departamento de Física, Universidad de Murcia, Apartado 4021, E-30080 Murcia, Spain*

(Received 31 January 2000; revised manuscript received 13 April 2000)

The effects of externally imposed stresses on the phase separation process of elastically coherent binary-alloy systems were investigated numerically with large-scale Langevin simulations. Both *two-* and *three-dimensional* systems were considered. The intrinsic crystallographic symmetries of the system compete with the external strains in the determination of both the shapes and the orientation of the precipitates. These can go all the way from the configurations predicted by a stress-free equilibrium criterion at small stresses, to lamellar and cylindrical configurations (or stripe configurations in two dimensions) at high stresses. Between these two extremes, there are new shapes and a continuous spectrum of orientation angles. This competition can also induce late-time, large-scale splitting of the domains. The stress effect is larger when the precipitates form the majority phase, and considerably smaller when they are in the minority.

I. INTRODUCTION

The mechanism behind Ostwald ripening, the late-stage processes by which a quenched binary-alloy system phase separates, was first explored theoretically by Lifshitz, Slyozov, and Wagner (LSW).¹ In the absence of any long-range interactions, growth is characterized by a single time-dependent quantity—the average domain size $R(t)$, which is predicted to follow a power-law growth $R(t) \sim t^n$ with a growth exponent of $n = 1/3$. Furthermore, the late-time morphology is self-similar in time, provided that one rescales both length and time scales in a proper manner,² which is reflected in spatial quantities such as the structure factor and domain morphology. Long-range forces can alter all of these kinetic characteristics. For example, in soft condensed-matter systems, such as lipid monolayers and block copolymer systems, effective long-range interactions can induce an inverse coarsening process in which material flows from the larger to the smaller droplets,³ and thereby stabilize both monodisperse and polydisperse droplet distributions.⁴ For binary alloy systems, elastic interactions constitute the most important set of effective long-range interactions. Such elastic interactions arise naturally from a lattice mismatch between the different atomic species, from differences in the elastic constants of the phases, and from externally imposed stresses. Experimentally, it is well known that elastic interactions alter the universal features of LSW growth. Typical phenomena associated with the phase separation of elastic binary-alloy systems include shape transformations, the quasi-ordering of the domains into spatially correlated structures, and deviations from the $n = 1/3$ growth law.^{5–14}

In two previous publications,¹⁵ hereafter referred to as SOSR I, we reported on large-scale two-dimensional (2D) and three-dimensional (3D) simulations of phase separation of model binary-alloy systems in the presence of long-range elastic fields appropriate for systems with a cubic symmetry. It was shown that aspects of the domain morphology, such as the orientation of the precipitates as well as the elastic

hardness/softness of the matrix relative to the precipitates, can all be understood in terms of a single selection criterion, which is based on the effective, weighted shear coefficients of the system. The mechanisms of phase separation were identified to be a combination of LSW growth and the elastically driven coalescence of the precipitates.

In this paper, we present a complementary numerical study of phase separation of elastically coherent binary-alloy systems in the presence of *external* stresses, thereby extending the work presented in SOSR I. Both 2D and 3D systems have been explored. In this case, the intrinsic crystallographic symmetries of the system now compete with the external strains in the determination of both the shapes and the orientation of the precipitates. These can go all the way from the configurations predicted by the stress-free selection criterion at small stresses, to lamellar and cylindrical configurations in three dimensions (stripes in two dimensions) at high stresses. Between these two extremes, there are new shapes and a continuous spectrum of orientation angles. The external stresses have the largest effect when the precipitates form the majority phase, and considerably less effect when they are in the minority. Moreover, the external stresses in competition with the crystallographic symmetries can also induce large-scale rearrangement of the domain morphology by “squeezing out” the matrix between the precipitates and inducing the splitting of domains.

Phase separation of elastically coherent binary alloys has been examined theoretically both with analytical theory and with different simulation techniques.^{16–27} However, because of the complexity of the equations and the high computational cost associated with the simulations, work has largely been confined to 2D, or to 3D systems with only a very small number of interacting droplets. Three-dimensional work is, however, important if a meaningful comparison between theory and experiment is to be made. This work, along with SOSR I, represents a first step in that direction. With the large-scale integration of a Langevin model, we have explored phase separation in the presence of externally imposed stresses.

II. MODEL AND SIMULATION

To investigate phase separation with elastic effects and externally imposed stresses, we use a Langevin model first introduced by Cahn²¹ and Onuki.^{19,22} The model assumes coherent interfaces, and incorporates the effects of anisotropic elasticity, elastic inhomogeneities between the different phases, and external strains. This phase-field model is formulated in terms of the order parameter field $\psi(\vec{\mathbf{x}}, \mathbf{t})$, the displacement fields $\mathbf{u}(\vec{\mathbf{x}}, \mathbf{t})$, and the elastic strain tensor $\mu_{ij} = 1/2(\partial u_i/\partial x_j + \partial u_j/\partial x_i)$. In dimensionless form, the free-energy functional is

$$F[\psi] = \int d\mathbf{x} [f(\psi) + \frac{1}{2}(\nabla\psi)^2 + \alpha\psi \text{Tr}(\mu) + f_{el}(\mu)], \quad (1)$$

where $f(\psi) = -\psi^2/2 + \psi^4/4$ denotes the bulk free-energy density; α is a parameter that couples the order parameter (concentration field) to the trace of the strain tensor—i.e., $\text{Tr}(\mu) = \nabla \cdot \mathbf{u}$, and f_{el} is the elastic free-energy density. For the specific case of a system with cubic symmetry, the elastic free-energy density becomes

$$f_{el} = \frac{\kappa}{2}(\nabla \cdot \mathbf{u})^2 + C_{44} \sum_{i \neq j} \mu_{ij}^2 + M \sum_i \left(\mu_{ii} - \frac{1}{d} \nabla \cdot \mathbf{u} \right)^2, \quad (2)$$

which is expressed in terms of the spatial dimension d , the compressibility modulus $\kappa = [C_{11} + (d-1)C_{12}]/d$ and shear moduli C_{44} , and $M = (C_{11} - C_{12})/2$. These parameters are written in terms of a set of dimensionless elastic coefficients C_{ij} , which in turn are related to the unscaled coefficients C_{ij}^* through the relation $C_{ij} = C_{ij}^* l / \sigma$, with l representing a characteristic length scale in the system such as the average domain size upon nucleation, and σ the surface tension. For elastically inhomogeneous alloys, the elastic coefficients may be partitioned in a convenient way with $C_{ij} = C_{ij}^o + C_{ij}' \tilde{\psi}$, where $\tilde{\psi}(\mathbf{r}, t) = \psi(\mathbf{r}, t) - \psi_o$ and ψ_o denotes the average value of the order parameter of the system. In this formalism, the stress tensor is defined as $\sigma_{ij} = \delta F / \delta \mu_{ij}$. Assuming that mechanical equilibrium is always maintained within the system, one readily obtains a set of nonlinear equations

$$\frac{\delta F}{\delta u_i} = \sum_j \frac{\delta \sigma_{ij}}{\delta x_j} = 0, \quad (3)$$

which relate the displacement and order parameter fields, i.e., to zeroth order,

$$\frac{\partial u_i}{\partial x_j} = A_{ij} - \frac{\alpha}{k_{lo}} \frac{\partial^2 W}{\partial x_j \partial x_i}, \quad (4)$$

where A_{ij} represents some constant external affine deformation, $k_{lo} = C_{12}^o + 2C_{44}^o$, and W is a potential function: $\nabla^2 W = \tilde{\psi}(\mathbf{r}, t)$. In order to effectively deal with the externally applied strain, it is convenient to introduce the symmetric tensor S_{ij} via

$$S_{ij} = \left[A_{ij} + A_{ji} - \frac{2}{d} \delta_{ij} \text{Tr}(A) \right] \frac{\kappa_{lo}}{\alpha}. \quad (5)$$

One can substitute these relations into Eq. (1), and carry out an expansion of the free energy to first order in C_{ij}' . This has the advantage of eliminating the displacement fields so that a free-energy functional formulated entirely in terms of ψ is obtained. The mathematical price that is paid for this elimination of variables is the introduction of an effective long-range interaction into the system via the potential function W . As this procedure has been detailed several times in the literature,^{19,22} we do not reproduce the steps here and simply cite the final result. The dimensionless, free-energy functional that is obtained after some tedious but straightforward algebra is

$$F_{eff}(\psi) = \int d\mathbf{x} \left[\frac{1}{2} |\nabla\psi|^2 + f(\psi) + f_{lr}(\psi) \right], \quad (6)$$

with an effective long-range interaction f_{lr}

$$f_{lr} = \mu_d \sum_{i \neq j} \left(\frac{\partial^2 W}{\partial x_j \partial x_i} \right)^2 + \mu_c \sum_i \left(\frac{\partial^2 W}{\partial x_i^2} - \frac{1}{d} \nabla^2 W \right)^2 + \sum_{ij} \varpi_{ij} \left(\frac{\partial \psi}{\partial x_i} \right) \left(\frac{\partial W}{\partial x_j} \right). \quad (7)$$

Here ϖ contains the contributions of the strains resulting from the externally imposed stresses, and is given by $\varpi = g_1 \mathbf{M}_1 + g_2 \mathbf{M}_2$, where

$$\mathbf{M}_1 = \begin{pmatrix} 0 & S_{xy} & S_{xz} \\ S_{xy} & 0 & S_{yz} \\ S_{xz} & S_{yz} & 0 \end{pmatrix}, \quad (8)$$

is a symmetric tensor dependent on the effective external shears only, and

$$\mathbf{M}_2 = \begin{pmatrix} S_{xx} & 0 & 0 \\ 0 & S_{yy} & 0 \\ 0 & 0 & S_{zz} \end{pmatrix}, \quad (9)$$

is a traceless tensor describing the externally imposed deformations along the principal axes. This free energy is described in terms of the two effective shear coefficients: $\mu_d = g_1 \tilde{\psi} + \tau_o$ and $\mu_c = g_2 \tilde{\psi}$, with $g_1 = C_{44}' (\alpha/k_{lo})^2$, $g_2 = (C_{11}' - C_{12}')/2 (\alpha/k_{lo})^2$, and $\tau_o = (2C_{44}^o + C_{12}^o - C_{11}^o) (\alpha/k_{lo})^2/2$. These terms are proportional to the square of the misfit ϵ , which is given by $\epsilon = -\alpha \Delta \psi / dk_{lo}$, where $\Delta \psi$ is the concentration difference between the matrix and the precipitates. The physics presented in this paper is a result of the externally imposed strains contained in the last term of the free-energy functional.

Since the free-energy functional is now entirely expressed in terms of ψ , the time-evolution of the order parameter following a quench is given by the Langevin equation

$$\frac{\partial \psi}{\partial t} = \nabla^2 \left(\frac{\delta F_{eff}}{\delta \psi} \right), \quad (10)$$

where we have neglected thermal noise.

To gain insight into the initial stages of spinodal decomposition with elastic fields and external strains, we have lin-

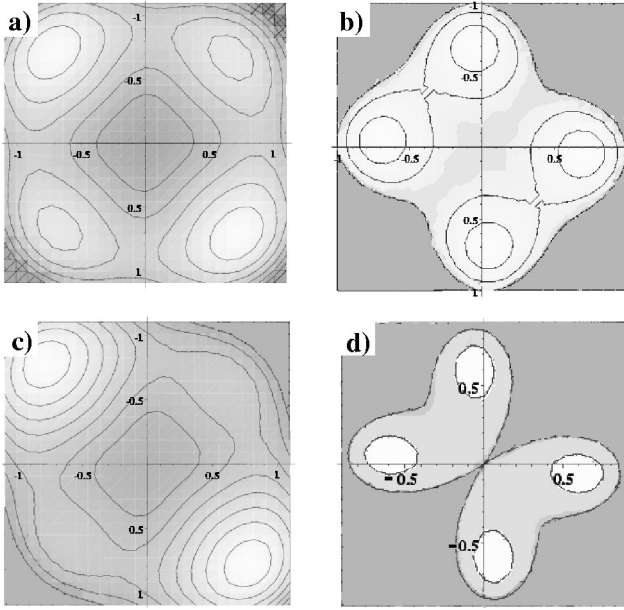


FIG. 1. Contour plots of 2D linear dispersion relation $\omega(k, \psi_o)$ with the unstable modes shaded in the lightest gray. Note that in the absence of any externally imposed strains, there are four lobes where the modes are unstable. These are centered either on the \hat{k}_x or \hat{k}_y axis, or on the diagonals. The effect of externally imposed strains is to change the shape of the unstable regions and to possibly reduce their number. Parameters for the different regions are (a) $\psi_o=0$, $(g_1, g_2, \tau_o)=(0.5, 0.5, 0)$ and $S_{xy}=1/16$, (b) $\psi_o=0$, elastic parameters $(0.5, 0, 0)$ and $S_{xy}=1/16$, (c) $\psi_o=0.3$, elastic parameters $(0.5, 1.0, 0.5)$, and $S_{xy}=1/4$, and (d) $\psi_o=0.3$, $(1.0, 0, 0)$ with $S_{xy}=1/16$.

earized the model. The linear equation of motion, $\partial \tilde{\psi}_k / \partial t = \omega(k, \psi_o) \tilde{\psi}_k$, is defined in terms of the Fourier transform of the order parameter, i.e., $\psi_k = \int d\mathbf{x} e^{i\mathbf{k} \cdot \mathbf{x}} \tilde{\psi}(\mathbf{x}, t)$, and the dispersion relation

$$\omega(k, \psi_o) = \gamma_k - \gamma_1 k^2 + \gamma_2 k^2 \sum_{i \neq j} \hat{k}_i^2 \hat{k}_j^2 + 2k^2 \sum_{i,j} \varpi_{ij} \hat{k}_i \hat{k}_j, \quad (11)$$

with $\gamma_k = k^2(1 - 3\psi_o^2 - k^2)$, $\gamma_1 = 2\mu_c(\psi_o)(1-d)/d$, $\gamma_2 = 2[2\mu_c(\psi_o) - \mu_d(\psi_o)]$, and $\hat{k}_i = k_i/k$. In the absence of any elastic effects ($g_1 = g_2 = \tau_o = 0$), the dispersion relation reduces to $\omega(k, \psi_o) = \gamma_k$, which is that of a pure model B system. In this case, the classical spinodal is located at $\psi_o = \pm 1/3$, and the maximally unstable mode is at $k^2 = (1 - 3\psi_o^2)/2$. In the dispersion relation, the terms with coefficients $\gamma_{1,2}$ result from the elastic misfits and inhomogeneities, while the last term represents the contribution of the external strains. The effects of the first three terms have previously been analyzed, with the following results. The γ_1 term does not break the circular symmetry of the modes in k space, but simply shifts the maximally unstable modes and the location of the spinodal. The γ_2 term breaks up the unstable region into four lobes (in two dimensions), which are centered either on the k_x and k_y axis or on the diagonals, depending on the specific elastic constants. Inclusion of the last term alters these unstable regions, as shown in Fig. 1. Note that in some cases, two out of four unstable lobes are

suppressed, indicating that configurations consisting of highly anisotropic domains all oriented in a similar direction are to be expected.

The Langevin equations were solved numerically using pseudospectral methods with Euler's method. Periodic boundary conditions were used on grids of size $(128)^2$, $(256)^2$ in two-dimensions, and $(64)^3$ and $(128)^3$ in three-dimensions, with mesh sizes of $dx=1.7$ and a timestep of 0.05 or less. The initial disordered state consisted of a Gaussian distribution of ψ 's centered about ψ_o with width of 0.1. The simulations were run on a Cray T90, with a typical $(128)^3$ run out to $t=10000$ requiring approximately 50 h.

III. RESULTS

We now present the results of our numerical simulations with an emphasis upon the domain morphology, the coarsening mechanisms, and the scaling properties of the structure factor. In addition to its four main parameters, i.e., volume fraction ψ_o , and effective elastic coefficients (g_1, g_2, τ_o) , whose effects were analyzed in SOSR I, the model is augmented by the S 's that specify the external strains. When quoting parameters for the various figures, we shall assume that all the S 's are zero, except for the values reported.

A. Morphology and microstructure

The most important effects of elastic fields on the phase separation of binary-alloy systems is to alter the microstructure of the precipitates. In the absence of any elastic interactions, the coarsening system forms either a bicontinuous structure consisting of two interpenetrating domains as is the case for a system with equal amounts of either phase, or a dropletlike morphology for systems with low volume fraction. In the presence of elastic interactions, but no external strains, it has previously been found that the morphology is determined by a single criterion, namely that *it is the matrix that holds most of the elastic distortions*. This then naturally leads to a selection criterion that is based on the *selection of the numerically smallest effective shear coefficient in the matrix weighted by the amount of precipitate present in the system*.¹⁵ This determines (i) which of two phases will form the matrix and/or precipitate, (ii) the hard versus soft nature of the phases, and (iii) the symmetry of the domains.

We find that the externally imposed stresses do not alter points (i) and (ii) of the selection criterion. Rather, the primary effect of the externally imposed stresses is to reorient the precipitates toward a single direction, and to alter their shapes. To illustrate these points, consider a 2D system. In absence of external strains, systems with both anisotropy and inhomogeneities would exhibit square domains oriented in the axial directions for the parameters (g_1, g_2, τ_o) as in Figs. 2(a,b,c,d,l); square domains oriented in the diagonal directions for (g_1, g_2, τ_o) in Figs. 2(e,f,k); and isotropic domains in Figs. 2(g,h,i,j). If the system were to be anisotropic but homogeneous, it would exhibit rectangular stripes distributed in equal proportions along perpendicular directions. Figure 2 shows new 2D configurations obtained by the addition of uniaxial strains ($S_{yy} = -S_{xx} \neq 0$ and $S_{xy} = 0$), shears ($S_{yy} = S_{xx} = 0$ and $S_{xy} \neq 0$), or a combination of both.²⁸ The addition of external strains tends to break the symmetry of the

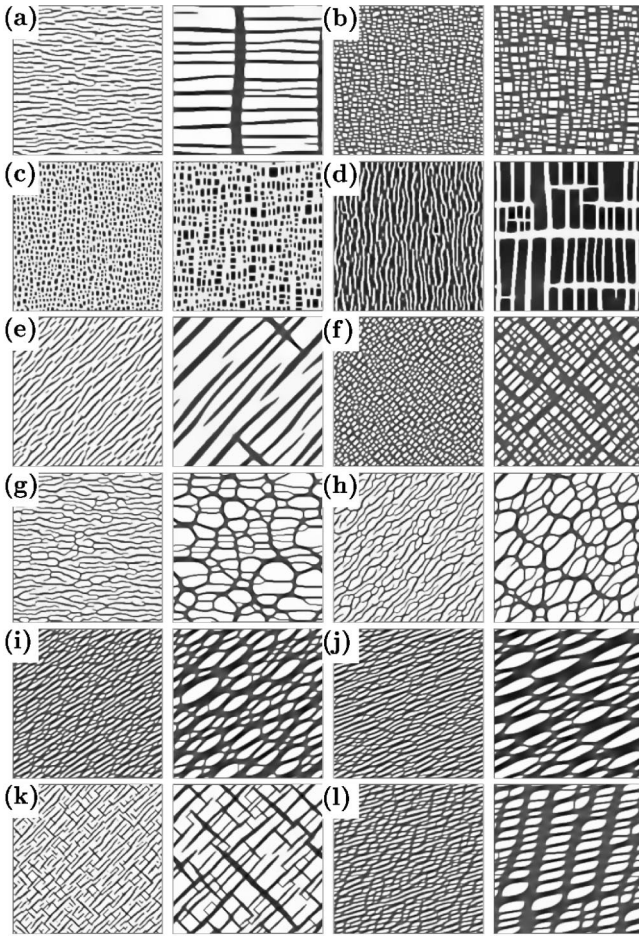


FIG. 2. Sample configurations for quenched 2D systems subject to external strains. The left and right panels are at time $t = 200, 10\,000$, respectively. Other parameters are given in Table I.

two perpendicular directions (whether axial or diagonal) favored by the selection criterion. The application of a uniaxial stress can produce alignment along the direction of the stress, or along the perpendicular direction, depending on the sign of the different elastic parameters. As shown in SOSR I, the most unstable direction, as determined by the linear stability criterion, does not necessarily coincide with the late-time orientation of the precipitates. Figures 2(a,b,c,d) show the effect of nonzero S_{ii} . In (a) and (b), with g_2 and S_{xx} having the same sign, the domains form rectangles elongated along the \hat{x} direction, while in (c) and (d), with g_2 and S_{xx} having the opposite sign, the rectangles are elongated along the \hat{y} direction. In general, when the external strains are moderate, the largest effect on the morphology occurs when the precipitates form the majority phase, as illustrated in Figs. 2(a,d,e). By contrast, there is relatively little effect when the precipitates form the minority phase, as illustrated in Figs. 2(b,c,f). In this case, the precipitates are all relatively small domains that appear barely elongated from the case of zero external strain. Figures 2(e,f) show the effect of pure shear, with domains elongating along the positive diagonal, i.e., $g_1 S_{xy} > 0$. Figures 2(g–j) illustrate the case of a system with isotropic elastic constants subject to external strains. In the absence of any external strains, these precipitates are initially rounded. At later times, they develop flat faces due to the close proximity of other precipitates. The effect of the

TABLE I. Parameters for Fig. 2.

Fig.	ψ_o	(g_1, g_2, τ_o)	Configuration without strain	S_{xx}	S_{xy}
(a)	0.3	(0,0.25,0)	white squares, axial	0.25	0
(b)	-0.3	(0,0.25,0)	white squares, axial	0.25	0
(c)	0.3	(0,-0.25,0)	black squares, axial	0.25	0
(d)	-0.3	(0,-0.25,0)	black squares, axial	0.25	0
(e)	0.3	(0.25,0,0)	white squares, diagonal	0.0	0.25
(f)	-0.3	(0.25,0,0)	white squares, diagonal	0.0	0.25
(g)	0.3	(0.25,0.25,0)	white isotropic domains	0.25	0
(h)	0.3	(0.25,0.25,0)	white isotropic domains	0.0	0.25
(i)	-0.3	(0.25,0.25,0)	white isotropic domains	0.5	1.0
(j)	-0.3	(0.25,0.25,0)	white isotropic domains	1.0	1.0
(k)	0.3	(0.125,0,-0.25)	white squares, diagonal	0	1/8
(l)	-0.3	(0.25,0.25,0.25)	white squares, axial	0.5	1.0

external strains is, again, both to distort and re-orient the precipitates. Thus, when the precipitates form the majority phase [Figs. 2(g,h)], they point in the \hat{x} and positive diagonal directions because the S_{xx} and S_{xy} terms dominate these specific simulations. In Fig. 2(k), both the selection criterion and the shear favor domains along the diagonal direction, but the domains are more broken up—when compared to Fig. 2(e)—along the perpendicular diagonal direction (this will be further discussed in Sec. B). Finally, Fig. 2(l) shows a combination of uniaxial and shear strains resulting in tilting from the preferred axial directions in the absence of external strains. (See also Table I.)

The external strains in Figs. 2(e,f,k) pick one of the two possible directions predicted by the selection criterion, while those in Figs. 2(g–j) determine the orientation of the domains without strong competition with the parameters (g_1, g_2, τ_o) , which would favor isotropy. Figure 2(l), on the other hand, shows the final result when two competing orientations are present. This competition is further illustrated in Fig. 3, where the orientation favored by (g_1, g_2, τ_o) competes with the orientation imposed by the external strains. The resulting shape and orientation of domains is a compromise between the two effects. Thus, when the external stress is small, then there is little effect on the square/axial configuration. Increasing the stress results in more deviations from this configuration: the domains become more rhomboidal, and the angle between their orientation and the axial directions increases. At very high stress, the precipitates completely deform into stripes oriented along the positive diagonal direction. Similar results are obtained for systems with diagonal symmetry subject to transformations along the axial directions.

A different case illustrating elastic competition is presented in Fig. 4, which show the behavior of systems for which the selection criterion predicts a change in morphology based solely on a change in the volume fraction. For these two systems, $(g_1, g_2, \tau_o) = (0.5, -0.5, 0)$ so that orientation of the domains is expected to change from diagonal to axial as ψ_o changes from +0.3 to -0.3 (from top to bottom). Indeed that is what is observed both in the absence and presence of external stresses¹⁵. However, the external stresses again induce significant shape changes in the domains. Thus,

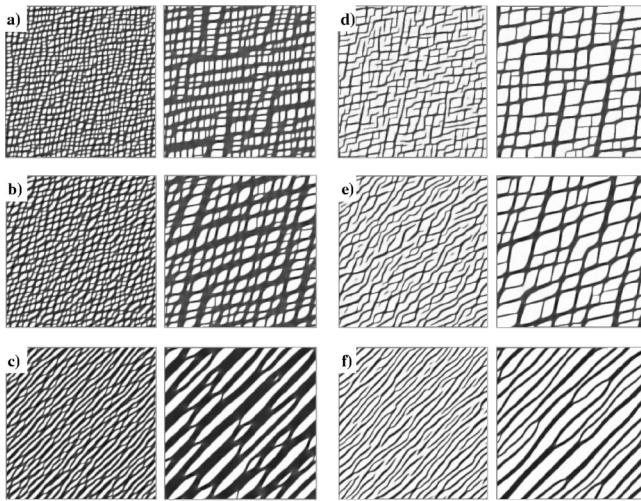


FIG. 3. Sample 2D configurations showing the case of a direct competition between the symmetry imposed by the selection criterion [elastic parameters (0.125,0.25,0.25) so that the selected orientation is axial], and an externally imposed shear, which favors the diagonal direction. The dominant effect of this competition is to tilt the domain walls of the precipitates in the direction of the imposed stress, and ultimately melt the domain's diagonal stripes. Panels (a)–(c) are for $\psi_o = -0.3$, (d)–(f) for $\psi_o = 0.3$. The external shear parameters S_{xy} are (a) 0.5, (b) 1.0, (c) 2.0, (d) 0.5, (e) 1.0, and (f) 2.0, respectively.

when a shear $S_{xy} = 0.5$ is imposed [Figs. 4(a,c,e)], the domains for $\psi_o = 0.3$ elongate along the positive diagonal, and will ultimately evolve so as to form rectangles similar to Fig. 2(e). When $\psi_o = -0.3$, the shear is not strong enough as to obliterate the axial configuration favored by the selection criterion in the absence of external strain; a rhomboidal shape emerges as a compromise. The counterpart situation occurs in Figs. 4(b,d,f), where a uniaxial stress is imposed. The results are largely reversed in that the dominant effect is

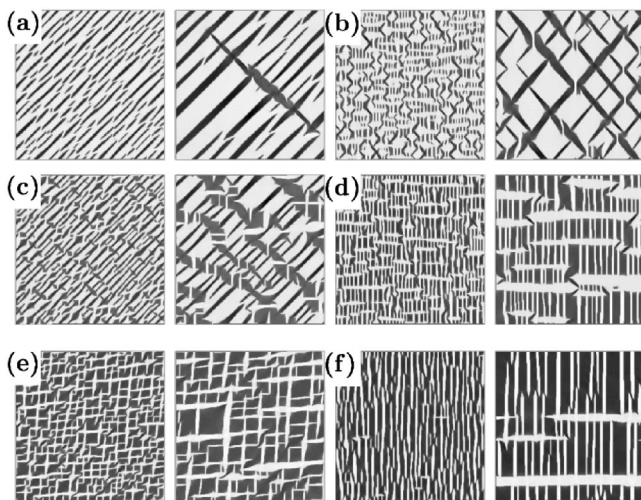


FIG. 4. Sample 2D configurations for systems with elastic parameters (0.5,-0.5,0) subject to external shear at times $t=400$, 10 000 showing change in morphology as a function of ψ_o : (a) and (b) $\psi_o = 0.3$, (c) and (d) $\psi_o = 0$, and (e) and (f) $\psi_o = -0.3$, where external strain is $S_{xy} = 0.5$ for (a), (c), (e) and $S_{xx} = 0.5$ for (b),(d),(f).

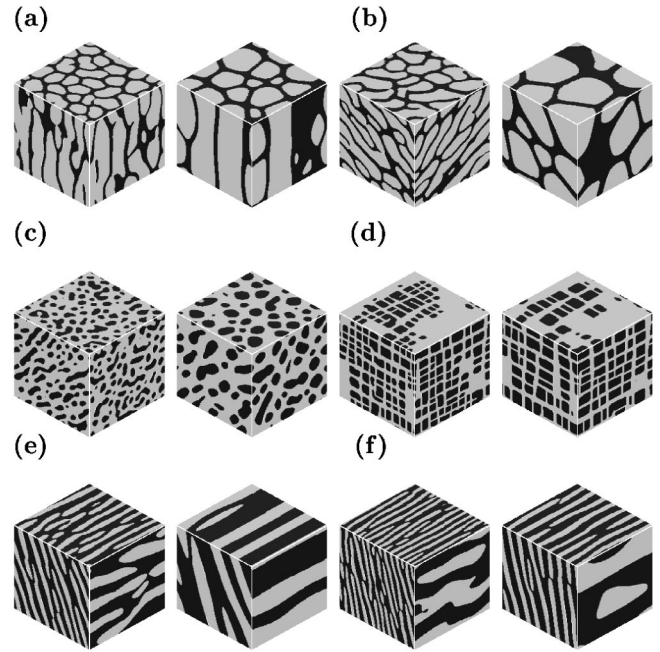


FIG. 5. Sample configurations for quenched 3D systems subject to external strains. The left and right panels are at times $t=400$, 10 000 for all systems except for (c) and (f), which are at times $t=200$, 1000; also $\psi_o = 0.3$, except for (e) and (f), for which $\psi_o = -0.3$. Elastic parameters of the system are (a) (0.5,0.5,0) $S_{xx} = S_{zz} = 1/9$ and $S_{yy} = -2/9$; (b) (0.5,0.5,0) $S_{xy} = S_{yz} = 1/8$; (c) $(-0.25,0,0)$ $S_{xy} = 1/8$; (d) (0.24,-0.8,0.7) $S_{xy} = 0.083$ and $S_{yz} = -0.083$; (e) (0.25,0.25,0) $S_{xx} = 1.5$, $S_{yy} = -0.5$, $S_{zz} = -1.0$ and $S_{xy} = 1.0$; (f) (0.25,0.25,0.5) $-S' s$ same as (e).

on the $\psi_o = -0.3$ configuration (bottom), rather than the $\psi_o = 0.3$ case (top), which preserves the diagonal orientation (with rhombi instead of squares). Clearly, the effects of the external stresses manifest themselves most readily when the external strains reinforce the orientation determined by the selection criterion.

Three-dimensional simulations show similar results for the domain morphologies. The 3D systems without externally imposed stresses display isotropic, “diagonal” ($(110) \times [1\bar{1}0]$ shears) and axial ($(100)[010]$ shears) symmetries. External stresses alter the morphologies in different fashions. For instance, for the case of isotropic elastic constants, the addition of a uniaxial strain changes the morphology so that the domains become more “cylinderlike” (when the strains are high enough), with facets due to the proximity of other domains. In this case, the domains align themselves along the appropriate axis [Fig. 5(a)], while for the case of shears, the plane in which the domains align themselves is tilted as shown in Fig. 5(b). Note that in this case, the external strains are not strong enough so as to induce lamellarlike domains as in Fig. 5(f). As in the 2D case, the effect of the external strains is most pronounced when the precipitates form the majority. For example, Fig. 5(c) shows a case where the precipitate forms the minority phase. In this case, the domain morphology is virtually unchanged. Another interesting example is given in Fig. 5(d). In the absence of external stresses, the morphology consists of a series of highly anisotropic domains pointing in the axial directions. Adding shears breaks up these highly anisotropic domains into a

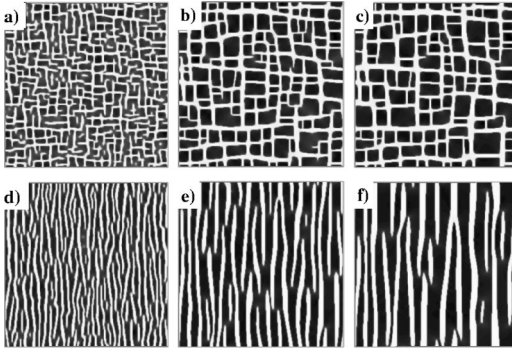


FIG. 6. Sample 2D configurations with parameters: $\psi_o = -0.3$ (g_1, g_2, τ_o) = (0, -0.25, 0) in the absence of external stresses for (a)–(c) and in the presence of external stresses $S_{xx} = 0.5$ for (d)–(f). The panels (a,d), (b,e) and (c,f) show times $t = 200, 1600, 5000$, respectively.

large number of smaller cubic domains. Finally, Figs. 5(e,f) show examples of systems with a mixture of elastic coefficients with both nonzero $\mathbf{M}_{1,2}$ (where the parameters used amount to a uniaxial strain, and two shears: one given by $S_{xy} \neq 0$ and one given by $S_{zz} = -S_{yy}$ and $S_{xx} = 0$). Without strains, the configuration in Fig. 5(e) would consist of isotropic domains and the configuration in Fig. 5(f) of cubic domains. The late-time morphologies show a series of tilted, sheetlike domains.

In summary, the external strains, while not altering the relative hardness/softness of the matrix with respect to the precipitates, introduce a continuous way of tuning the shape and orientation of the domains. These can go all the way from the configurations predicted by the selection criterion at small stresses, to lamellar and cylindrical configurations at high stresses, with a wealth of shapes and a continuous spectrum of orientation angles in between.

B. Growth of precipitates

In this section, we discuss the growth of the precipitates as a function of time, and the breakdown of dynamic scaling of the structure factor. As previously discussed in SOSR I, the phase-separating system evolves in such a way as to decrease both its interfacial and elastic free energy. This is achieved through a combination of LSW growth plus coalescence. Coalescence events dominate the ordering process when the precipitates form the majority phase. It gives rise to accelerated rates of growth with considerable deviations from the $n = 1/3$ growth law, i.e., the system coarsens faster than a pure model *B* system without any elastic effects. By contrast, when the precipitates form the minority phase, coalescence events are relatively infrequent, and the system displays a decreased rate of growth that is however consistent with a LSW exponent of $n = 1/3$. The coarsening rates can also be determined by elastically-induced chemical potential barriers.

When external stresses are relatively small, this qualitative picture does not change. For these cases, the plots of the average domain size $R(t)$ as a function of time largely resemble those of SOSR I, and need not be further considered here. However, two new features emerge when the stresses are significant. First, as already mentioned, the externally

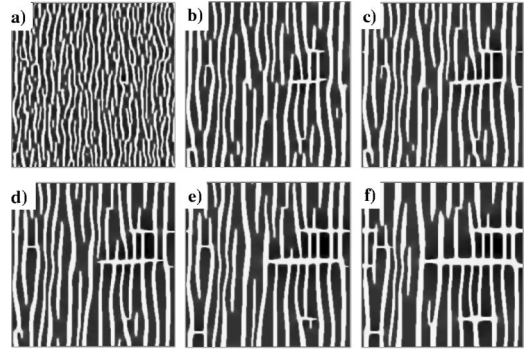


FIG. 7. Sample 2D configurations, with parameters and times as in the previous figures. However, now we have external stresses specified by $S_{xx} = 0.25$ and at times $t = 200, 1600, 2000, 2400, 3200, \text{ and } 5000$.

imposed stresses distort the precipitates, so that they are elongated and all are oriented in a single direction. If this distortion is large enough, then the domains distort to form ordered lamellar or cylindrical patterns (or stripes) broken up by defects, so that it is the annealing away of these defects that dominates the ordering process. Second, the competition between the intrinsic elastic symmetries and the external stresses can induce the large-scale splitting of the domains.

These features are illustrated in Figs. 6–8. Figures 6(a–c) show an example of a system without any external strains, and elastic parameters such that $\psi = +1$ forms the minority matrix phase with the precipitates aligned in the axial directions. Note that the features of the system are degenerate with respect to the two principal axes, i.e., no specific feature is associated with the \hat{x} and/or \hat{y} directions, respectively. Now, in Figs. 6(d–f) and 7, external stresses are imposed in the systems. For both systems, g_2 and S_{xx} have the opposite sign, and, therefore, the domains align along the \hat{y} direction (vertical). The main difference between Figs. 6(d–f) and Fig. 7 is that the strain in Fig. 7 is half the (absolute) value of that in Figs. 6(d–f). Thus, Figs. 6(d–f) show smooth stripes aligned in the elastically soft direction, whereas the corresponding stripes in Fig. 7 are split or cut up. This is a direct consequence of the competition introduced by the cubic symmetry of the system, which—under a smaller value of the strain—reasserts itself. Similar features are observed in

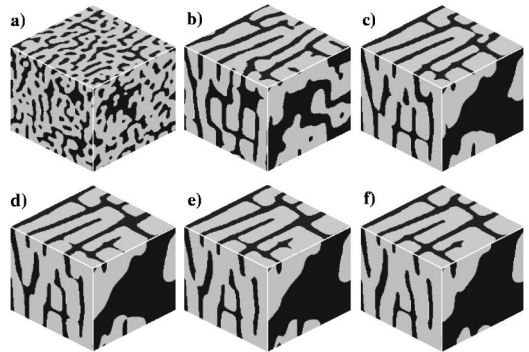


FIG. 8. Sample 3D configurations showing domain splitting. System parameters are $\psi_o = 0.3$ (g_1, g_2, τ_o) = (0, 0.25, 0), and $S_{xx} = 1/16$, $S_{yy} = -1/16$. Panels (a)–(f) are at times $t = 200, 1000, 2000, 2400, 2600, \text{ and } 3000$, respectively.

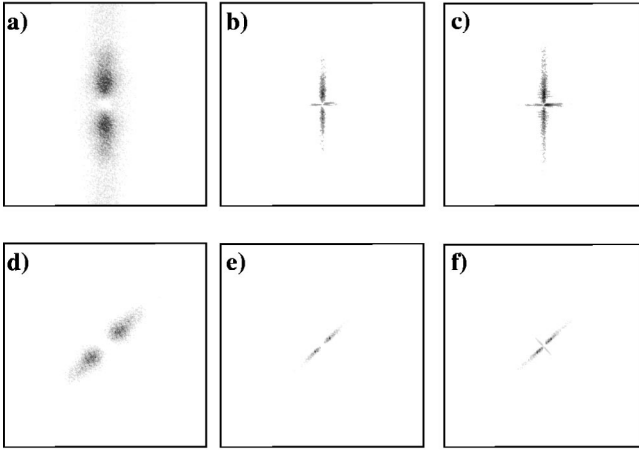


FIG. 9. Sample 2D structure factors $S(k_x, k_y)$ as a function of time, showing its highly anisotropic character when external stresses are present. Parameters of the system: for (a)–(c), $\psi_o = 0.3$, with $(g_1, g_2, \tau_o) = (0, 0.25, 0)$ and $S_{xx} = 0.25$ at times $t = 200, 5000, 10\,000$, respectively; for (d)–(f), $\psi_o = 0.3, (0.25, 0, 0)$ and $S_{xy} = 0.25$ at similar times. In the first case, the scattering is oriented primarily along the k_y and k_x axis (not shown); in the second case, the dominant scattering is along the positive diagonal.

3D, as illustrated in Fig. 8. Moreover, the stripelike pattern in Fig. 7 is broken up by dislocations and disclinations, and evolves slowly to eliminate these defects. In many ways, the morphology of the system resembles that of phase-ordering fluids under external shears. The splitting of domains in Figs. 7 and 8 can be viewed as nucleation of perpendicular stripes of matrix. That is, at the very early times, the stress effects dominate while the nucleation of perpendicular matrix stripes occurs in much longer time scales. Eventually, the configuration ends in an array of rectangles, which is the compromising equilibrium configuration resulting from the competition between the intrinsic elastic symmetries and the external stresses. Using this criterium, we can also compare Figs. 2(e) and 2(k). In the absence of external stresses, the equilibrium configuration in both cases is an array of squares distributed symmetrically along the diagonal directions. Figure 2(k) has a smaller shear S_{xy} and a higher absolute value of the shear diagonal coefficient in the matrix: $\mu_d = g_1 \tilde{\psi} + \tau_o [-0.338$ in Fig. 2(k) and -0.175 in Fig. 2(e)]. Therefore, the domains in Fig. 2(k) are more broken up than those in Fig. 2(e), where the external strain is more dominant.

These morphology changes are reflected in both the structure factor and changes in the average domain size, as illustrated in Figs. 9 and 10. First, the highly anisotropic nature of the configurations is evident when one examines the structure factor, shown in Fig. 9. In the absence of any elastic effects, the structure factor consists of a diffuse ring that brightens and shrinks in diameter as the phase separation proceeds. In the presence of externally imposed stresses, there is no ring, but rather two peaks that mark the dominant orientation of the domains. These peaks are located either on the \hat{k}_y axes [Figs. 9(a–c)] or on the positive diagonal [Figs. 9(d–f)], depending on the elastic parameters of the system. In addition, Figs. 9(a–c) show the development of two further peaks, which are significantly smaller in size, which are oriented along the k_x axes. The development of these sec-

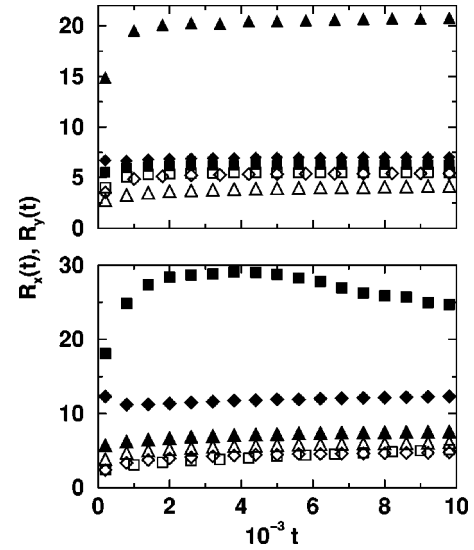


FIG. 10. Sample behavior of R_x (filled symbols) and R_y (open symbols) for elastically isotropic systems: for the top panel, the parameters are $\psi_o = 0.3$ (g_1, g_2, τ_o) = (0.25, 0.25, 0) with increasing shears S_{xx} as stripes develop; squares, 0.05; diamonds, 0.1; and triangles, 0.5; and for the bottom panel, the parameters as in Fig. 6(b) for changing concentration are squares, $\psi_o = 0.3$; diamonds, $\psi_o = 0.0$; and triangles, $\psi_o = -0.3$. Note that the system has been rotated such that \hat{x} corresponds to the positive diagonal.

ondary peaks may be understood in terms of a reassertion of the original domain symmetry, which is otherwise dominated by the externally imposed stresses. The first three panels of Fig. 9 correspond to a morphology that is similar to Fig. 7, so that the development of these secondary peaks may be associated with the nucleation and growth of the stripes of matrix that cut across the domains. In contrast, Figs. 9(d–f) correspond to a case with similar features as Figs. 6(d–f). In this case, all of the stripes are oriented in a single direction, so that there is no significant development of secondary peaks.

To probe the growth of domains, we have calculated the first moment of the structure factor resolved in each of the principal directions. Essentially, we calculated $R_{x,y,z} = \pi/k_{x,y,z} \langle k_{x,y,z} S(\vec{k}, t) \rangle$, where $S(\vec{k}, t)$ is the structure factor (not averaged), and the angular brackets denote an average over the configurations.² In situations where the principal axis of the system did not correspond to \hat{k} axes, the structure factor was first rotated by the appropriate angle. Typical behaviors are shown in Fig. 10. For instance, consider the case of configurations under increasing stresses so as to ultimately form stripes, as shown in the upper panel of Fig. 10. Initially, the values of R_x and R_y are close together in value. However, as the external stress increases, and the domains progressively elongate, the R_x component increases while the R_y component remains almost constant. This is characteristic of the formation of stripes. The lower panel of Fig. 10 corresponds to the configurations shown in Fig. 4, with the axes rotated such that the positive diagonal corresponds to the \hat{x} direction. The most interesting case here corresponds to Fig. 4(a) for which $\psi_o = 0.3$. Initially, the system forms stripes that are oriented along the diagonal directions, so that R_x shows a very sharp, initial increase. Hence, there is a large

difference in the R_x and R_y values, as already seen in Fig. 9. However, at some point, we see the nucleation of a stripe of matrix oriented along the negative diagonal that begins to cut the domains. As more and more of the matrix is squeezed out from between the precipitates and ends up oriented along the negative diagonal, there is a corresponding decrease in the value of R_x and a corresponding increase in R_y . In other words, the system displays inverse coarsening behavior.⁴

Finally, we have examined the issue of dynamic scaling of the structure factor. Since under the influence of the externally imposed stresses each of the directions grows (shrinks) at a different rate, some care must be taken in implementing the scaling. As the most general case, we examined

$$S(\vec{k}, t) = R_x(t)R_y(t)R_z(t)F(x_1, x_2, x_3),$$

where $x_1 = k_x R_x(t)$, $x_2 = k_y R_y(t)$, $x_3 = k_z R_z(t)$, and F is a time-independent shape function. Clearly, this formula reduces to the usual case $S(k, t) = R(t)^d F(x)$ when the R_i 's are equal. The main results are as follows. In cases where the precipitate forms the minority phase, and the influence of the externally imposed stresses are relatively small, good scaling similar to that reported in SOSR I is obtained.¹⁵ However, there appears to be no dynamic scaling in the other situations. This is particularly true for cases when the domains undergo large-scale shape transformations to form lamellas or cylinders.²⁹

IV. SUMMARY

In summary, we have investigated the phase separation of model 2D and 3D binary-alloy systems with externally im-

posed elastic stresses with Langevin simulations. We find that the selection criterion for the *phase* of the matrix/precipitates, as discussed previously in SOSR I, is unchanged. However, the symmetry of the domains can no longer be predicted by this criterion. The intrinsic crystallographic symmetries of the system compete now with the external strains in the determination of both the shapes and the orientation of the precipitates. These can go all the way from the configurations predicted by the stress-free selection criterion at small stresses, to lamellar and cylindrical configurations in three dimensions (stripes in two dimensions) at high stresses. Between these two extremes, there are new shapes (i.e., rhomboidal and elliptical shapes in two dimensions) and a continuous spectrum of orientation angles. The stripes or lamellas created when the precipitates run together at large stresses form quasicrystalline configurations broken up by defects that evolve very slowly in time. The external stresses have the largest effect when the precipitates form the majority phase, and considerably less effect when they are in the minority. The external stresses in competition with the crystallographic symmetries can also induce large-scale rearrangement of the domain morphology by inducing massive splitting of the domains. As expected, the highly anisotropic nature of the domain morphology is reflected in the structure factor of the system, which generally does not display late-time scaling.

ACKNOWLEDGMENTS

This work was supported by NSF Grants Nos. DMR-95000858, POWRE-9870464, and PB96-1120 DGICyT, Spain. We also thank the North Carolina Supercomputing Center (NCSC) for significant amounts of Cray T90 support.

-
- ¹I. M. Lifshitz and V. V. Slyozov, *J. Phys. Chem. Solids* **19**, 35 (1961).
- ²C. Roland and M. Grant, *Phys. Rev. Lett.* **60**, 2657 (1988); **63**, 551 (1989); *Phys. Rev. B* **39**, 11 971 (1989).
- ³M. Seul and C. A. Murray, *Science* **262**, 558 (1993); M. Seul, *J. Phys. I* **4**, 319 (1994).
- ⁴C. Sagui and R. C. Desai, *Phys. Rev. Lett.* **74**, 1119 (1995); *Phys. Rev. E* **52**, 2822 (1995).
- ⁵A. J. Ardell, R. B. Nicholson, and J. D. Eshelby, *Acta Metall.* **14**, 1295 (1966); A. Maheshwari and A. J. Ardell, *Phys. Rev. Lett.* **70**, 2305 (1993); M. Meshkimpour and A. J. Ardell, *Mater. Sci. Eng., A* **185**, 153 (1994); J. Wimmel and A. J. Ardell, *ibid.* **183**, 169 (1994); A. B. Kamora, A. J. Ardell, and C. N. Wagner, *Metall. Mater. Trans. A* **27A**, 2888 (1996); J. H. Cho and A. J. Ardell, *Acta Mater.* **45**, 1399 (1997).
- ⁶B. v. Grossmann, H. Biermann, S. Mechsner, and H. Mughrabi, *Mater. Adv. Power Eng., Proceedings of the 6th Liege Conference*, edited by J. Lecomte-Beckeres *et al.* (Schriften des Forschungszentrum, Jülich, 1998), Vol. 5, Pt. 3, p. 1429; H. Muchrabi, in *The Johannes Weertman Symposium*, edited by R. J. Arsenault *et al.* (The Minerals, Metals, and Materials Society, Warrendale, PA, 1996), p. 267; H. Mughrabi, W. Schneider, V. Sass, and C. Lang, in *Strength of Materials*, edited by Oikawa *et al.* (Japan Inst. Metals, Sendai, Japan, 1994), p. 705.
- ⁷T. Miyasaki, K. Nakamura, and H. Mori, *J. Mater. Sci.* **14**, 1827 (1979).
- ⁸L. A. Bendersky, P. W. Voorhees, W. J. Boettinger, and W. C. Johnson, *Scr. Metall.* **22**, 1029 (1988).
- ⁹W. Hein, *Acta Metall.* **37**, 2145 (1989).
- ¹⁰H. Calderon and G. Kostorz, in *Neutron Scattering for Materials Science*, edited by S. M. Shapiro, S. C. Moss, and J. D. Jorgensen, MRS Symposia Proceedings No. 166 (Materials Research Society, Pittsburgh, 1990), p. 210.
- ¹¹A. Maheshwari and A. J. Ardell, *Scr. Metall. Mater.* **26**, 347 (1992).
- ¹²H. A. Calderon, G. Kostorz, Y. Y. Qu, H. J. Dorantes, J. J. Cruz, and J. G. Cabanas-Moreno, *Mater. Sci. Eng., A* **238**, 13 (1997).
- ¹³A. Ges, O. Fornaro, and H. Palacio, *J. Mater. Sci.* **32**, 3687 (1997).
- ¹⁴P. Fratzl, F. Langmayr, G. Vogl, and W. Miekeley, *Acta Metall. Mater.* **39**, 753 (1991); F. Langmayr, P. Fratzl, G. Vogl, and W. Miekeley, *Phys. Rev. B* **49**, 11 759 (1994).
- ¹⁵C. Sagui, D. Orlikowski, A. Somoza, and C. Roland, *Phys. Rev. E* **58**, R4092 (1998); D. Orlikowski, C. Sagui, A. Somoza, and C. Roland, *Phys. Rev. B* **59**, 8646 (1999).
- ¹⁶J. D. Eshelby, *Prog. Solid. Mech.* **2**, 89 (1961); J. K. Lee, D. M. Barnett, and H. I. Aaronson, *Metall. Trans. A* **8**, 963 (1977).
- ¹⁷A. G. Khachaturyan, *Theory of Structural Shape Transformations in Solids* (Wiley, New York, 1983).
- ¹⁸W. C. Johnson and J. W. Cahn, *Acta Metall.* **23**, 1839 (1984); W. C. Johnson and P. W. Voorhees, *J. Appl. Phys.* **61**, 1610 (1987);

- I. M. Kaganova and A. L. Roitburd, Zh. Éksp. Teor. Fiz. **94**, 156 (1988) [Sov. Phys. JETP **67**, 1173 (1988)]; A. G. Khachaturyan, S. V. Semenovskaya, and J. W. Morris, Acta Metall. **36**, 1563 (1988); W. C. Johnson, M. B. Berkenpas, and D. E. Laughlin, *ibid.* **36**, 3149 (1988); K. Kawasaki and Y. Enomoto, Physica A **150**, 463 (1988); Y. Enomoto and K. Kawasaki, Acta Metall. **37**, 1399 (1989); T. Miyazaki and M. Doi, Mater. Sci. Eng., A **110**, 175 (1989); W. C. Johnson and P. W. Voorhees, Solid State Phenom. **23**, 87 (1992).
- ¹⁹A. Onuki, J. Phys. Soc. Jpn. **58**, 3065 (1989); **58**, 3069 (1989); H. Nishimori and A. Onuki, Phys. Rev. B **42**, 980 (1990); A. Onuki and H. Nishimori, J. Phys. Soc. Jpn. **60**, 1 (1991); Phys. Rev. B **43**, 13 649 (1991); H. Nishimori and A. Onuki, J. Phys. Soc. Jpn. **60**, 1208 (1991).
- ²⁰M. E. Thompson, C. S. Su, and P. W. Voorhees, Acta Metall. Mater. **42**, 2107 (1994).
- ²¹J. W. Cahn, Acta Metall. **9**, 795 (1961); **10**, 179 (1962).
- ²²C. Sagui, A. Somoza, and R. C. Desai, Phys. Rev. E **50**, 4865 (1994).
- ²³Y. Wang, L. Q. Chen, and A. G. Khachaturyan, Scr. Metall. Mater. **25**, 1387 (1991); Acta Metall. Mater. **41**, 279 (1993).
- ²⁴J. Gayda and D. J. Srolovitz, Acta Metall. **37**, 641 (1989).
- ²⁵J. K. Lee, Scr. Metall. Mater. **32**, 559 (1995).
- ²⁶P. Fratzl and O. Penrose, Acta Metall. Mater. **43**, 2921 (1995).
- ²⁷C. A. Laberge, P. Fratzl, and J. L. Lebowitz, Phys. Rev. Lett. **75**, 4448 (1995).
- ²⁸In two dimensions, these two cases are actually the same, as a simple rotation can transform systems with $S_{ii} \neq 0/S_{xy} = 0$ into $S_{ii} = 0/S_{xy} \neq 0$. This is not the case in three dimensions.
- ²⁹This result must be qualified. The theory for phase separation predicts the emergence of a single length scale even in the presence of elastic fields, so that dynamic scaling is expected. However, we do not find evidence for this in our simulations. This may well be due to the finite length and time scales of the currently feasible simulations.